We are IntechOpen,
the world's leading publisher of
Open Access books
Built by scientists, for scientists

4,800
Open access books available

122,000
International authors and editors

135M
Downloads

Our authors are among the

154
Countries delivered to

TOP 1%
most cited scientists

12.2%
Contributors from top 500 universities

BOOK CITATION INDEX
CLARIVATE ANALYTICS
INDEXED

WEB OF SCIENCE™

Selection of our books indexed in the Book Citation Index
in Web of Science™ Core Collection (BKCI)

Interested in publishing with us?
Contact book.department@intechopen.com

Numbers displayed above are based on latest data collected.
For more information visit www.intechopen.com

Mechanical and Electronic Properties of Graphene Nanostructures

Ricardo Faccio, Luciana Fernández-Werner, Helena Pardo,
Cecilia Goyenola, Pablo A. Denis and Álvaro W. Mombrú
Centro NanoMat, DETEMA, Polo Tecnológico de Pando, Facultad de Química,
Cryssmat-Lab, DETEMA, Facultad de Química,
CINQUIFIMA, Espacio Interdisciplinario,
Universidad de la República, Facultad de Química,
Uruguay

1. Introduction

Quite recently a new carbon nanostructure, called graphite nanoribbon (GNR), has emerged, taking the attention of the scientific community because of its promising use in spintronics. It is manly attributed to the work of Son et al. (Son et al. 2006 a; Son et al. 2006 b), who predicted that in-plane electric field, perpendicular to the periodic axis, induces a half-metal state in zigzag nanoribbons (ZGNR). This state corresponds to a one spin flavour with metallic behaviour, while the opposite spin flavour experiences an increase in the energy gap. Apart from the interesting dependence of the electronic structure upon an electric field, this is a promising material for future spintronic devices, since it could work as a perfect spin filter. Very recently Campos-Delgado et al. (Campos-Delgado et al. 2008) reported a chemical vapour deposition route (CVD) for the bulk production of long, thin, and highly crystalline graphene ribbons (less than 20-30 µm in length), with widths from 20 to 300 nm and small thicknesses (2 to 40 layers). In addition, the bottom up synthesis of these nanostructures may be feasible as noted by Hoheisel and collaborators (Hoheisel et al. 2010). This experimental advance further increases the expectations for the use of these materials in high-tech devices. In parallel there is an increased interest in the physical properties of carbon nanostructures in general, due to their outstanding mechanical and electronic properties. Recently, Lee et al. (Lee et al. 2008) measured the mechanical properties of a single graphene layer, demonstrating that graphene is the hardest material known, since the elastic modulus reaches a value of 1.0 TPa. Besides, many efforts have been dedicated to study the electronic properties of graphene, because creating a gap could allow the use of graphene in field effect transistors. Many mechanisms have been proposed with that purpose: nano-pattering, creating quantum dots, using multilayer, doping with heteroatoms such as sulphur (Denis et al. 2009), covalent functionalization (Bekyarova et al. 2009) and applying mechanical stress (Pereira et al. 2009; Gui et al. 2008). Recently Gui (Gui et al. 2008) proposed that graphene under a symmetrical strain distribution always leads to a zero band-gap semiconductor, and the pseudogap decreases linearly with the strain strength in the elastic linear regime. However, asymmetrical strain induces an opening of

band gaps at the Fermi level. The evidence presented above clearly points that it is important to know how the electronic properties of ZGNR depend on stress, in order to predict its performance in future devices (e.g. gates). The bibliography shows a few works related with the study of strain in graphene nanoribbons (Sun et al. 2008; Xu et al. 2009; Su et al. 2008), neither of them informing the Young's modulus of GNR. The main conclusions from those works indicates that there is no important variation of the electronic properties of zigzag nanoribbons upon stress-strain effects (i.e. energy gaps and local magnetic moments), while there is no information regarding the mechanical properties of this nanostructure. Recently our group (Faccio et al. 2009) presented the first systematic determination of the Young's modulus, Poisson's ratio and calculated Shear modulus for graphene nanoribbons.

1.1 Theoretical background

The Young's modulus can be considered a measure of the stiffness of a solid. It is widely used for isotropic and continuous media, in which, the elastic parameters together defines the mechanical properties of the material. These parameters are: the Young's modulus E^{3D}, the shear modulus G and the Poisson's ratio υ. These three parameters are related by simple expressions that allows the calculation of one of them if two are known. For a three dimensional (3D) solid they can be defined as:

$$E^{3D} = \frac{\sigma_x}{\varepsilon_x} = \frac{1}{V_0}\left(\frac{\partial^2 E_S}{\partial \varepsilon_x^2}\right)_{E_0} \tag{1.1}$$

$$G^{3D} = \frac{\sigma_{xy}}{\varepsilon_{xy}} = \frac{1}{V_0}\left(\frac{\partial^2 E_S}{\partial \varepsilon_{xy}^2}\right)_{E_0} \tag{1.2}$$

$$\upsilon = -\frac{\varepsilon_y}{\varepsilon_x} = -\frac{\varepsilon_z}{\varepsilon_x} \tag{1.3}$$

$$G^{3D} = \frac{E^{3D}}{2(1+\upsilon)} \tag{1.4}$$

The Young's modulus represents the ratio between the uniaxial stress σ_x and the uniaxial strain ε_x, and can be easily calculated in terms of the strain energy E_S, the tensile strain ε_x, and the equilibrium volume V_0. The shear modulus is also defined in terms of the shear components of the strain and stress tensors. Finally, the Poisson's ratio υ relates the axial strain ε_x with the transversal strain ε_y or ε_z.

In the case of graphene it has more sense to define the in-plane stiffness instead of the classical 3D Young's modulus, because of the reduced dimensionality of this material. For this reason in graphite the elastic properties can be considered independent of the interlayer distance between graphene layers, c_0=3.35 Å, and the constants can be described as follows:

$$E^{2D} = \frac{1}{A_0}\left(\frac{\partial^2 E_S}{\partial \varepsilon_x^2}\right)_{E_0} = E^{3D}c_0 \tag{2.1}$$
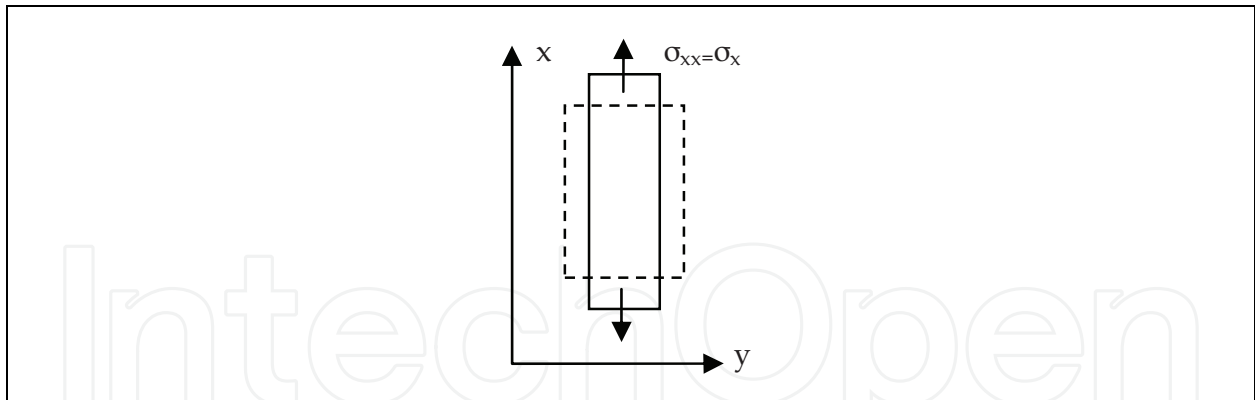
Fig. 1. Lateral contraction produced by an axial stress

$$\upsilon = -\frac{\varepsilon_y}{\varepsilon_x} = -\frac{l_0}{w_0}\frac{\partial w}{\partial l} \tag{2.2}$$

where A_0 corresponds to the equilibrium reference area of the 2D material, with length l_0 and width w_0. The in-plane stiffness of graphite is obtained considering an axial load applied over graphene. The value obtained in this case is $E^{3D}=1.02(3)$ TPa (Blakslee et al. 1970). It allows us to obtain $E^{2D}= 3.41(9)$ TPaÅ. This value is almost the same as that the one obtained experimentally for graphene, $E^{2D}=3.42(30)$ TPaÅ (Lee et al. 2008) using nano indentation with atomic force microscope. This result is in agreement with those reported by Kudin et al. (Kudin et al. 2001) and Van Lier et al. (Lier et al. 2000). Using *Ab initio* methods they reported Young's modulus of $E^{3D}= 1.02$ TPaÅ (Kudin et al. 2001) and 1.11 TPaÅ (Lier et al. 2000). The Poisson's ratio is unambiguously defined in terms of the transversal ratio over the longitudinal variation with a value of $\upsilon= 0.149$.

Some reports based on another theoretical approach; using Brenner potentials, show wide scattered results, with strong dependence on the equilibrium adjustment yield used in the calculation (Reddy et al. 2006). The results obtained by this method correspond to Young's modulus of $E^{3D}=0.7$ TPa and 1.11 TPa, with Poisson's ratio of $\upsilon=0.40$ and 0.25, with the use of modified and non-modified potential respectively. Many representative results, based on Reddy et al. (Reddy et al. 2006), are presented in Table 1.

Single-walled carbon nanotubes (SWCNT) are an example of a one dimensional system described in terms of 2D property E^{2D}, since two parameters must be informed, the tube length (L) and the tube radius (r), in order to gain independence of size effects. Several expressions have been published for their mechanical properties in terms of multidimensional Young's modulus as: E^{3D}, E^{2D}, etc (Wu et al. 2008, Bogár et al. 2005). The values reported show a wide variation on experimental E^{nD}'s values, up to an order of magnitude of difference. This is mainly due to the difficulty in determining the precise structure of nanotubes under study, the presence of defects, chirality, etc. Recently, Wu et al. (Wu et al. 2008) used a combined optical characterization of individual SWCNT, coupled with magnetic actuation technique, to measure the Young's modulus of nanotubes with known chirality. The Young's modulus obtained was $E^{3D}=0.97(16)$ TPa, assuming a wall thickness of c=3.4 Å corresponding to the interlayer spacing in graphite. No dependence on the nanotube's chiral index within the experimental accuracy was found. This result agrees quite well with theory, in particular with the values reported by Bogár et al. (Bogár et al. 2005). Employing an all electron DFT method, they reported E^{2D} for different tubes radius,

Reference	E^{3D} (TPa)	υ	Remarks
	Graphene		
Kudin et al. 2001	1.02	0.149	Graphene (*Ab initio*)
Lier et al. 2000	1.11	-	Graphene (*Ab initio*)
Reddy et al. 2006	1.012	0.245	Graphene (Brenner**)
Reddy et al. 2006	0.669	0.416	Graphene (Brenner*)
Arroyo et al. 2004	0.694	0.412	Graphene (Brenner)
Reddy et al. 2005	1.11	0.45	Graphene (Truss model)
Faccio et al. 2009	0.96	0.17	Graphene (*Ab initio*)
	Carbon Nanotubes		
Zhang et al. 2002	0.694	-	SWNT (Brenner)
Lu et al. 1997	0.97	0.28	SWNT (Empirical model)
Shen et al. 2004	0.213–2.08	0.16	SWNT (MM)
Yu et al. 2000	0.32–1.47	-	SWNT (Experiments)
Sammalkorpi et al. 2004	0.7	-	SWNT (MD)
Yoon et al. 2005	1.0	0.25	DWNT (Vibrations)
Wu et al. 2008	0.81–1.13	-	SWNT (Experiments)
Bogár et al. 2005(***)	0.8-1.05	-	SWNTS (*Ab initio*)
Bogár et al. 2005	1.05	-	SWNT (5,5) - (*Ab initio*)
Faccio et al. 2009	1.01	-	SWNT (5,5) - (*Ab initio*)

(*) Minimized potential and (**) Non-minimized Potential

(***) This result was converted to E^{3D} for comparison purposes, using: $E^{3D}=E^{2D}c_0$.

Table 1. Representative results for different carbon nanostructures.

that ranges from r=1.32 Å to 4.11 Å. They concluded that there is no dependence between the Young's modulus and the chirality of the nanotube.

1.2 Electronic and geometrical structure of graphene nanoribbons

In graphene nanoribbons, the presence of different types of boundary shapes, called edges, modifies the electronic structure of the material. The major effects are observed at the Fermi level, displaying unusual magnetic and transport features (Palacio et al. 2005). There are two typical shapes for graphite edges, with quite opposite consequences, zigzag and armchair. The zigzag edges present electronic localized states at the boundaries, corresponding to non-bonding states that appear at the Fermi level as a large peak in the density of states. It gives rise to important effects on the magnetic and transport properties of nanographite. These localized states are totally absent in the case of armchair edges. For these reasons the more interesting case correspond to nanographite with zigzag edges.

A graphite nanoribbon consists of strips of graphene; it is created by cutting the sheet along two parallel lines. The direction of these lines defines the type of edge, while the distance between them defines its width. This kind of structures was first introduced by Fujita et al. (Fujita et al. 1996; Nakada et al. 1996; Wakabayashi et al. 1999) who studied its electronic structure using tight-binding models over graphite. They found that the typical diamagnetic ordering of graphene is disrupted because of the presence of zigzag edges, as mentioned earlier, that breaks the delocalized π-bands creating an instability that is resolved via electronic spin polarization; see Figure 2(b). In order to study size and edge effects in carbon nanoribbons Fujita & Wakabayashi (Palacio et al. 2005) proposed a simple model that consists in N dimmers that establish the nanoribbon's width; the edges are terminated with
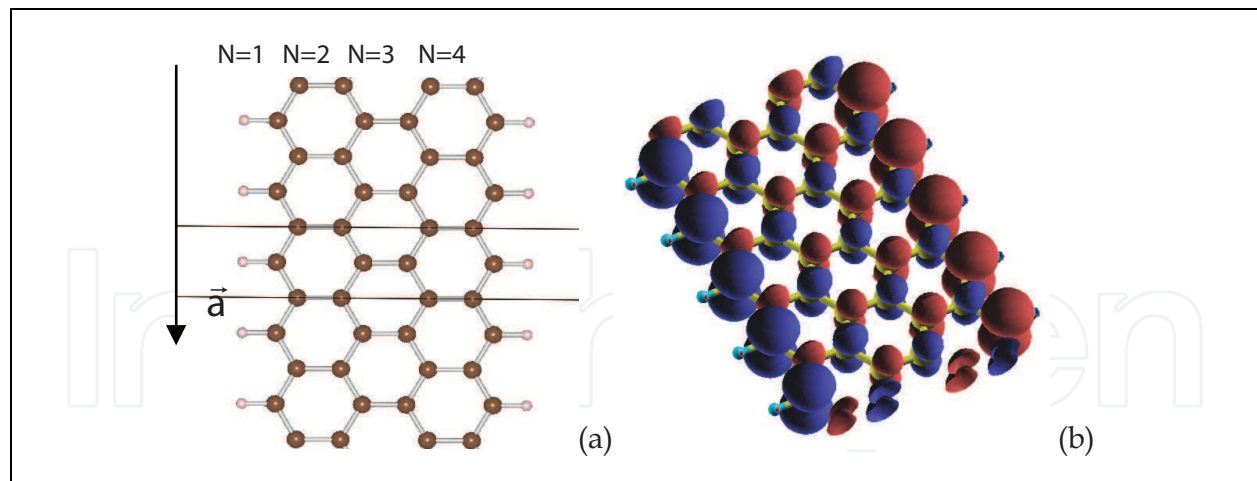
Fig. 2. (a) Graphite nanoribbon with N=4, displaying its smallest unit cell; the arrow shows the periodic direction $\vec{a}$. (b) Spin density map, showing the antiferromagnetic arrangement between opposite edges.

hydrogen atoms, while the translational invariance of graphene is kept along the direction perpendicular to the width, see Figure 2(a). Regarding the electronic structure, the non-magnetic solution has many states at the Fermi level, which produces a strong instability that can be resolved by spin polarization or geometrical distortion. Due to the non-bonding character of the zigzag localized edge states, the geometrical reconstruction is unlikely to happen (Miyamoto et al. 1999) and another mechanism should be explored for this purpose. The other alternative mechanism consists in a spin polarization of the electronic density, in particular with an antiparallel arrangement between near carbon atoms, with a zero total magnetization. The local magnetic moments increase at the edges; they couple oppositely with their near neighbours carbon atoms, and damp inwards the ribbons. Since opposite carbon atoms at the edges always belong to different sublattices the net magnetization is zero. Another important consequence of the spin polarization of the electronic density is the aperture of a gap in ZGNR, yielding a Slater insulator (Pisani et al. 2007). The opening of the gap is related with the ZGNR width, since it is a consequence of the interaction between edges. For this reason wider ribbons, with longer distances between opposite edges, recovers the graphene geometry with a gap equal to zero. The tendency observed corresponds to an exponential decay of the energy gaps when increasing the nanoribbon's width (N). Table 2 shows the results for N=4, 5, 6, 7, 8, 9 and 10.

Width (N)	Energy Gap (eV)
4	0.63
5	0.59
6	0.54
7	0.50
8	0.46
9	0.43
10	0.40

Table 2. Energy gaps for different zigzag graphene nanoribbons

The antiferromagnetic arrangement is always the ground state, having lower energy than the nonmagnetic and ferromagnetic solution. The ferromagnetic solution refers to a local

ferrimagnetic arrangement, but with equal polarization between opposite carbon atoms at the edges, with a non-zero magnetic moment. The electronic structure of N=4 ZGNR is shown in Figure 3, where the band structure is presented together with the corresponding density of states.
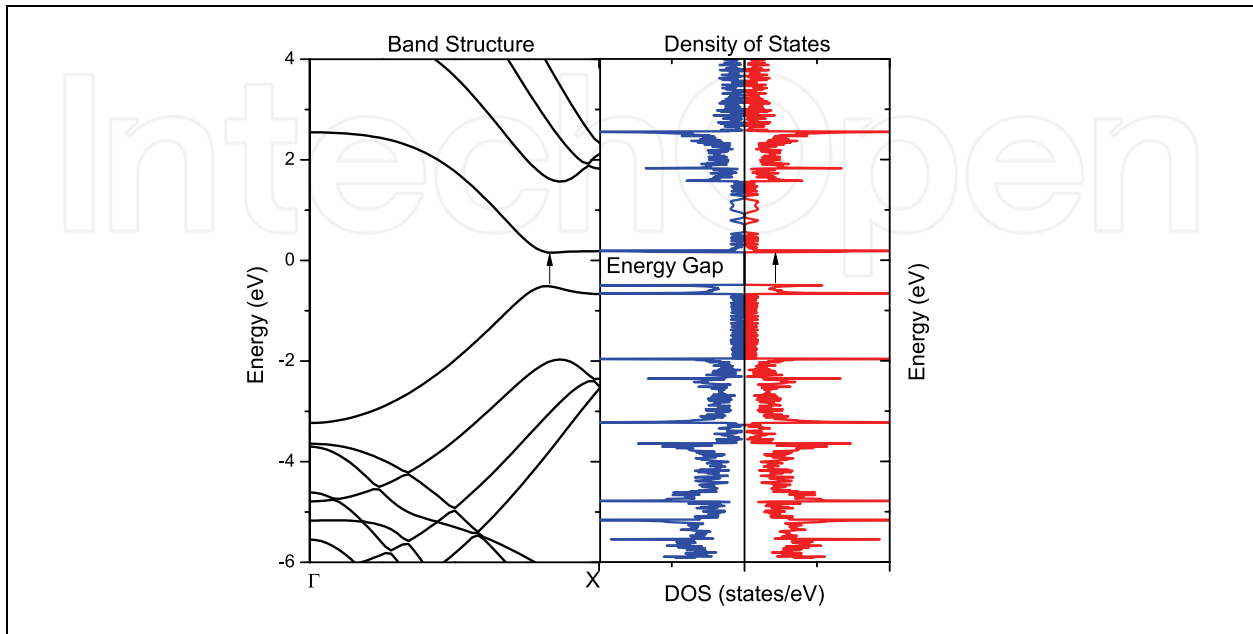

Fig. 3. Band structure along the periodical path Γ-X, and the corresponding total density of states for the N=4 zigzag graphite nanoribbon.

Recently the scientific community has revitalized the attention in GNR not only from the theoretical standpoint, but for the promising of its technological applications. It is manly attributed to the work of Son et al. (Son et al. 2006 a; Son et al. 2006 b) who predicted that in-plane electric field, perpendicular to the periodical axis, induces a half-metal state in ZGNR. This state corresponds to a one spin flavour with metallic behaviour; while the opposite spin flavour experiences an increase in the energy gap. Apart of the interesting dependence of the electronic structure upon an electric field, this is a promising material for future spintronic devices, since it could work as a perfect spin filter. Figure 4 shows the case of N=4 ZGNR where different electric fields were applied obtaining a half-metal state for an E=0.8 eV/Å.

2. Methods

2.1 Density functional theory

There exist many methodologies for obtaining the electronic structure of many-particle systems. "Density Functional Theory (DFT)" (Hohenberg et al. 1964; Kohn et al. 1965) is a way to study the electronic structure of many-particle systems with a relative low computational cost, since the description of a quantum system is based in functionals that depends on the electronic density instead of the many-particle wave functions. It is the corner stone of the theory, since the complexity of solving the many-particle wavefunction decreases and we only must deal with a set of almost single-electron-wavefunctions instead. In this way the Hamiltonian of the many-particle system, called Kohn-Sham Hamiltonian, can be described as:

$$E[\rho] = T_0[\rho] + V_{ee}[\rho] + V_{xc}[\rho] + V_{ext}[\rho] \qquad (3.1)$$

where T_0 corresponds to the kinetic energy functional, V_{ee} is the inter-electronic repulsion, V_{ext} is the external potential coming from the nucleus arrangement, and finally V_{xc} is the exchange and correlation potential. While T_0, V_H and V_{ext} can be easily incorporated in the Hamiltonian, since they are well know because of its universal expressions, the V_{xc} is not known in an exact form and must be estimated or approximated.

$$E[\rho] = T_0[\rho] + V_{ee}[\rho] + V_{xc}[\rho] + V_{ext}[\rho] \qquad (3.2)$$

The exchange and correlation effects must be incorporated in the equations because the universal functionals T_0 and V_{ee} do not take into account the fermionic behaviour of the electronic wavefunction, and fail to describe instantaneously electron-electron interactions, and it is attributed to the mean field form of the handled expressions. This justifies the incorporation of an additional term into the Hamiltonian, called the exchange-correlation potential V_{xc}, with the purpose to deal with the limitations early mentioned.

The incorporation of the V_{xc} term represents an additional problem, since there is no knowledge about the exact form of the functional and approximations should be made in order to estimate its value.
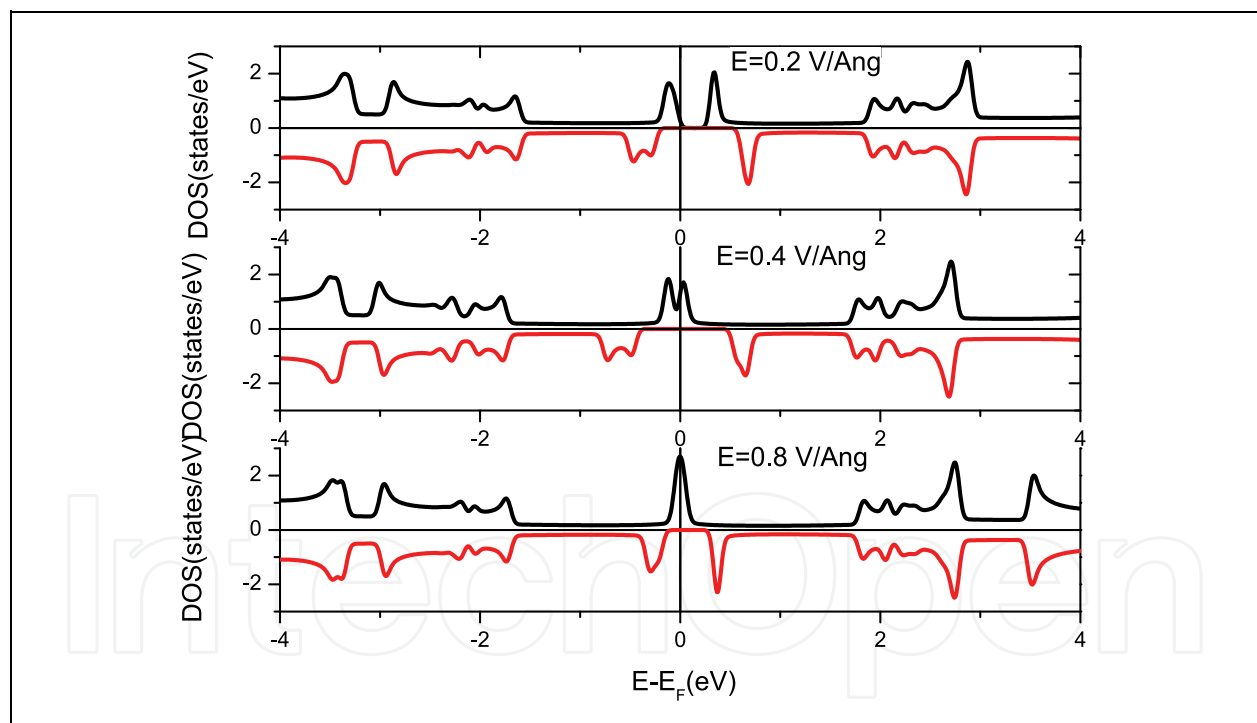

Fig. 4. Density of states for N=4 ZGNR under different applied electric fields (a) 0.2 V/Å, (b) 0.4 V/Å and (c) 0.8 V/Å.

2.2 Exchange-correlation functionals and dispersive interactions

The last section described the philosophy behind DFT and the origin of the exchange-correlation potential (xc-potential). The first and most widely used xc-potential is the so called "Local Density Approximation (LDA)" introduced by W. Kohn and L. J. Sham. The model assumes that the exchange-correlation energy of a particular density $\rho(r)$ can be

obtained with the help of the results obtained for an interacting homogeneous electron gas. The total density of the material is divided in infinitesimal portions of constant density $\delta\rho(r)$ each. Then the exchange correlation energy is added by an amount equal to the one corresponding to a uniform interacting electron gas of density $\rho_{EG}(r) = \delta\rho(r)$ that occupies the same piece of volume (Perdew et al. 1981; Ceperley et al. 1980). This model clearly neglects the fact that true densities are not homogeneous, but the results obtained are surprisingly good either for slowly varying or strongly varying densities either. The next step points towards the description of non homogeneous electron density, building a V_{xc} that accounts for the density of the neighbour pieces of volume. This is the Generalized Gradient Approximation (GGA), and because there is no a unique way to incorporate the density gradient in it, there exist many versions of this functional. While GGA gives better description of geometrical and electronic issues than LDA under particular circumstances (Konahoff et al. 2002), both systematically underestimate electronic band gaps, and generally tends to delocalise the electronic density. A possible solution to these problems consist in building hybrid xc-potentials that allow us to join the advantages of DFT and Hartree-Fock formalism together in one functional. Probably, the most widely used hybrid functional is called B3LYP (Becke et al. 1993; Lee et al. 1988; Vosko et al. 1980; Stephens et al. 1994). It is based on the original idea from Becke (Becke et al. 1993), where the functional is assembled with the correlation term suggested by Lee, Yang and Parr (LYP) (Lee et al. 1988), and the exchange term is a weighted sum of three terms that includes the Hartree-Fock term. The three empirical parameters were determined by fitting the predicted values to a set of atomization energies, ionization potentials, proton affinities, and total atomic energies (Stephens et al. 1994). Since B3LYP includes in some amount the Hartree-Fock exact-exchange this functional can be considerer as a non-local, and its implementation at the moment is done for localized basis set codes. This is main the reason why LDA and GGA are still widely used, including for Van der Waals materials, and the selection depends on the particular interest over the system under study.

While LDA, GGA and B3LYP functionals perform reasonably well describing metallic, covalent and ionic bonds; Van der Waals interaction is still a missing aspect within DFT implementations. This kind of binding is explained in terms of dynamical dipole-dipole correlations, which is inherently a non-local interaction and therefore neglected within LDA/GGA schemes. Recently there have been serious efforts to solve this problem with significant results (Khon et al. 1998; Rydberg et al. 2003; Dion et al. 2004). Román-Pérez (Román-Pérez et al. 2009) proposed an efficient implementation of the Van der Waals functional proposed by Dion (Dion et al. 2004) in the SIESTA code (Ordejón et al. 1996; Soler et al. 2002), with really promising results. They found an overhead in total computational cost, in comparison with semilocal functionals, very moderate for medium and large systems. For these reasons LDA and GGA exchange-correlation functionals are still used for describing Van der Waals solids such as graphite. The use of one over the other depends on the physical property to be assessed. LDA is widely used for graphite simulations since it gives good geometrical parameters and energy differences, in particular the calculated interlayer distance between graphene seems to be in good agreement with experiment (Tournus et al. 2005; Charlier et al. 1994). At first, would seem that LDA describes quite well the Van der Waals interactions in graphite, but what really happens is a fortuitous cancellation of errors (Tournus et al. 2005). A detailed analysis shows that the electron density determined by the LDA method is not adequate, offering a poor description of the

topology of the electron density in particular in the direction perpendicular to graphene (Strocov et al. 2000).

Moreover GGA xc-potential offers better geometrical reconstruction in the graphene plane, with better C-C distances (Konstantinova et al. 2006; Zhang et al. 2007) and better in-plane phonon frequencies (Wirtz et al. 2004). Furthermore GGA reproduces qualitatively the corrugation of the crystal potential (Strocov et al. 2000), but the energy involved in the $\pi\cdots\pi$ interactions is totally underestimated, leading to an increase of the interlayer distance of c_{GGA}=8.20 Å which is about 20% higher than the corresponding experimental value c_{GGA}=6.70 Å (Trucano et al. 1975). This is the main reason why LDA is preferred over GGA, when $\pi\cdots\pi$ interactions are involved. Thus the results of these approximations can be interpreted as the upper and lower bound for the interaction strength.

2.3 Basis Sets and DFT codes for *Ab initio* simulations

Ab initio methods can be selected in terms of the basis set used to generate the KS orbitals. The more representative methods correspond to plane wave expansion and localized basis sets. Each method has its advantages and pitfalls. The plane-wave methods are the most accurate within DFT. They are asymptotically complete allowing for systematic convergence and offering for spatially unbiased wave-functions. The main disadvantage is the computational cost, since many wave-functions per atom are needed for a good accuracy. Additionally the methods led to very high total energies, thus energy differences are very small and thus sensitive to the converged basis set. On the other hand the localized basis sets are in general very efficient, since the number of basis functions per atom is very small, reducing the computational cost. The physical interpretation of many properties is straightforward, since the basis sets are based on atomic like functions. In difference to plane waves methods localized basis set shows systematic lack for convergence and previous knowledge is needed for an accurate treatment of the basis sets.

2.4 Simulation of carbon nanoribbons

The theoretical study of the uniaxial stress on different ZGNR is based on the First Principles – Density Functional Theory (Hohenberg et al. 1964, Kohn et al. 1965) which we successfully used to study, bulk graphene, thioepoxidated SWCNTs and sulfur doped graphene (Denis et al. 2009; Faccio et al. 2008; Denis et al. 2008). The simulations are performed using the SIESTA code (Ordejón et al. 1996; Sánchez-Portal et al. 1997; Soler et al. 2002) which adopts a linear combination of numerical localized atomic-orbital basis sets for the description of valence electrons and norm-conserving non-local pseudopotentials for the atomic core. The pseudopotentials were constructed using the Trouiller and Martins scheme (Troullier et al. 1991) which describes the interaction between the valence electrons and atomic core. We selected a split-valence double-ζ basis set with polarization orbitals for all the carbon atoms. The extension of the orbitals is determined by cutoff radii of 4.994 a.u. and 6.254 a.u. for s and p channels respectively, as obtained from an energy shift of 50 meV due to the localization. The total energy was calculated within the Perdew–Burke–Ernzerhof (PBE) form of the generalized gradient approximation GGA xc-potential (Perdew et al. 1996 (a), 1997 (b)). The real-space grid used to represent the charge density and wavefunctions was the equivalent of that obtained from a plane-wave cutoff of 230 Ry. The atomic positions were fully relaxed in all the cases using a conjugate-gradient algorithm (Press et al. 1986) until all forces were smaller than 10 meV/Å was reached. A Monkhorst Pack grid

(Monkhorst et al. 1976) of 300x2x2 supercell, defined in terms of the actual supercell, was selected to obtain a mesh of 600 k-points in the full Brillouin Zone. All these parameters allow the convergence of the total energy. In order to validate our methodology we calculated the Young's modulus of (5,5) SWCNT, for which the literature shows several results from *Ab initio* methods (see Table 1). The smallest unit cell contains a total of 20 carbon atoms. With the purpose to study the dependence on the number of carbon atoms, we simulated the case 40 carbon atoms per unit cell. The Young's modulus obtained are $E^{3D}=1.03(2)$ and $E^{3D}=1.01(3)$ TPa, for 20 and 40 carbon atoms in the unit cell respectively. The results are consistent within the uncertainty which was estimated from the variance obtained from the adjustment of the second order fitting of the energy upon unitary deformation. Therefore one can conclude that the results are not affected by the number of supercells used, in particular along the periodic direction. Additionally the results are in good agreement with the reported in the bibliography see Table 1, in particular with an excellent agreement with those from Bogár et al. (Bogár et al. 2005). Regarding geometry in graphene nanoribbons, we can distinguish two C-C bond orientations: the bond perpendicular to the crystalline periodic direction d(|) and the bond diagonal to the normal direction d(/). The bond distances differ from the inner part of the ribbon (bulk) respecting the atoms at the edge. In the case of bulk C-C distances we found d(|)bulk= 1.44 Å and d(/)bulk=1.44 Å, while at the edge of the ribbon we found d(|)edge= 1.46 Å, and d(/)edge=1.43 Å. This result agrees with the tendency observed by Pisani et al. (Pisani et al. 2007), where the perpendicular bond elongates at the edge, contracting the corresponding diagonal bond at the edge. It promotes an increase of the zigzag C-C-C angle from 120° at the bulk to 121.9° at the edge. This trend is observed for the whole un-stressed studied ribbons. For all of these reasons, we can unequivocally conclude that our methodology is valid.

3. Results and discussion

The selected ZGNR for simulation correspond to N=4, 5, 6, 7, 8, 9 and 10. Since the code handled was designed for three dimensional materials, we designed special unit cells. All the cells were orthogonal, with the GNR placed in the ab plane, and oriented with the periodic direction along the *a* axis, see Figure 1 for the ZGNR N=4 sketch. In order to avoid interference between symmetry images, vacuum regions of 15 Å were added along *b* and *c* directions. In the case of the smallest unit cell, the *a* axis value for every cell is approximately a_0= 2.495 Å, with a total number of atoms of 2N+2. With the purpose of increase the number of degrees of freedom in each case, the cells were expanded in four units along the *a* axis ($a=4a_0$), it allows us to multiply by four the number of atoms inside the supercells according to 8N+8. The total number of atoms in each case is: 40, 48, 56, 64, 72, 80 and 88. The stress-strain curves are obtained applying different stress to the GNR, allowing full atomic relaxation together with full unit cell parameters optimization, until the desired stress tensor is reached. Since we are considering uniaxial strain only, the Voigt tensor has only one non-zero component: $[\sigma_x, \sigma_y, \sigma_z, \sigma_{xy}, \sigma_{xz}, \sigma_{yz}] \rightarrow [\sigma_x, 0, 0, 0, 0, 0]$. The selected stress components of the Voigt tensor allow us to establish strains in the range of ε_x= ±0.020 for the whole series, which assures a linear stress regime (Liu et al. 2007, Khare et al. 2007). It corresponds to a quadratic dependence of the total energy upon the strain. The most important features of the data treatment are presented in Figure 5 for N=10 ZGNR.
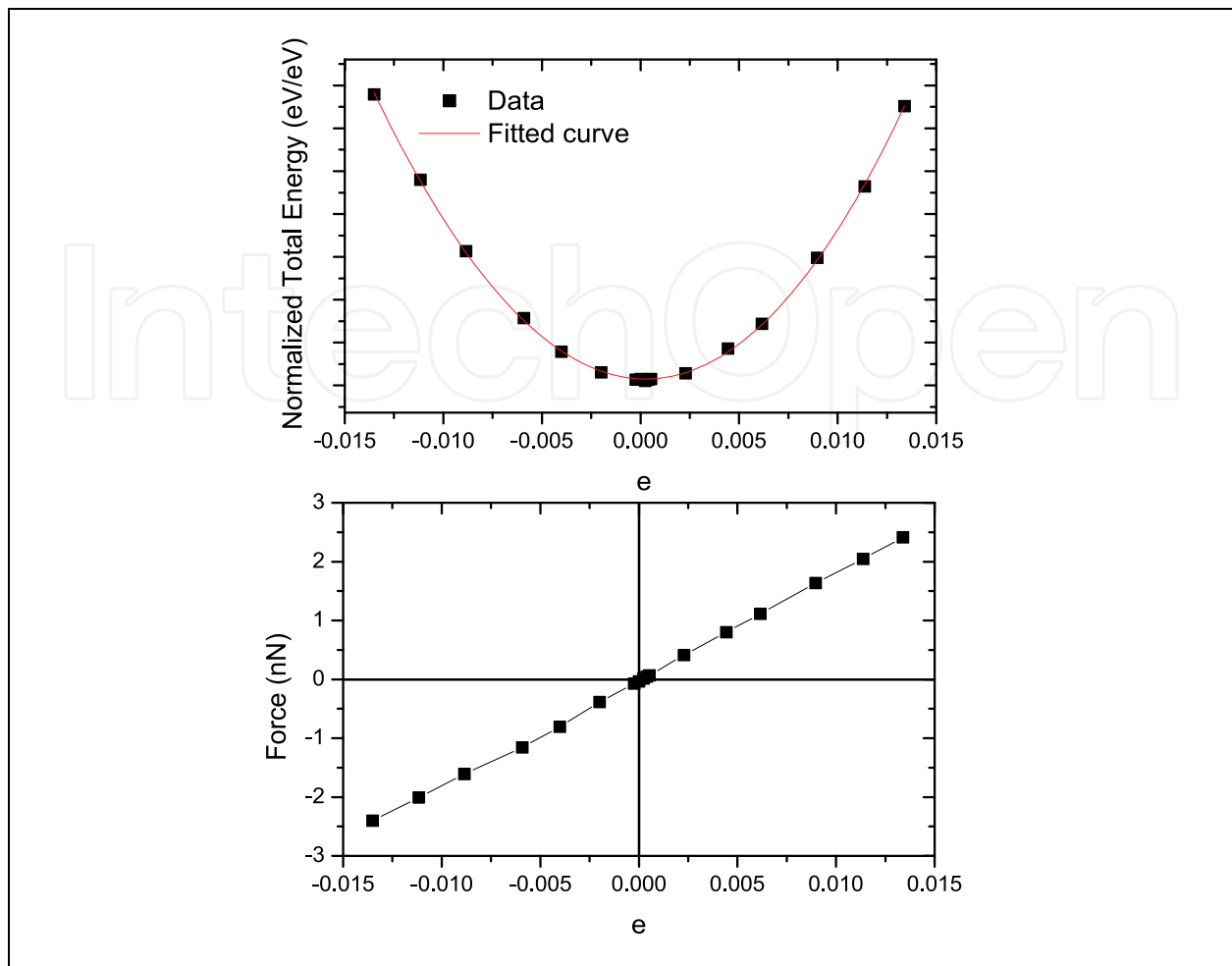
Fig. 5. Normalized total energy versus strain, and the corresponding force versus strain for N=10 ZGNR (Faccio et al. 2009).

While the second derivative of the total energy is easily obtained, the reference surface is ambiguously defined, with a dependence of the results upon the surface selection. In particular, the problem arises with the selection of the GNR's width, since it is a surface of pruned edges. In our case we have selected two different ways of determine the reference width of GNR: the shortest C-C width (d_A) and the longest C-C width (d_B). A sketch of these distances is presented in Figure 6(a). It is clear that neither of them are the best selection, and it becomes a problem when we want to compare these results in the N-infinity limit, corresponding to graphene. For this reason all the results are presented, together with the results for graphene. Figure 6(b) shows the variation of the E^{2D} upon the GNR's width N. The same results are presented in Table 3. To check the reliability of the calculations, the case of N=∞ (graphene) was studied. In this case we take a rectangular supercell with 32 carbon atoms. Each periodic crystalline axis were oriented along the zigzag and armchair directions, selecting a c value of 20 Å in order to avoid interference between images. The stress was applied along the zigzag axis. The obtained Young's modulus $E^{3D}=E^{2D}/c_0=$ 0.964(9) TPa agrees quite well with early reported values (see Table 1), as well as the Poisson's ratio $\upsilon = 0.17$, that matches with the one reported by Kudin et al. (Kudin et al. 2001) $\upsilon=0.149$ and Liu et al. (Liu et al. 2007) $\upsilon=0.186$. It is another point that helps us to validate our methodology.

N	d_A	d_B	E^{2D}_A	E^{2D}_B
	Å		TPaÅ	
4	05.80	07.19	5.04	4.07
5	08.66	09.35	4.21	3.90
6	10.12	11.51	4.27	3.76
7	12.98	13.68	3.88	3.68
8	14.45	15.83	4.08	3.72
9	17.30	18.00	3.84	3.69
10	18.77	20.16	3.91	3.64
∞	-		3.23	

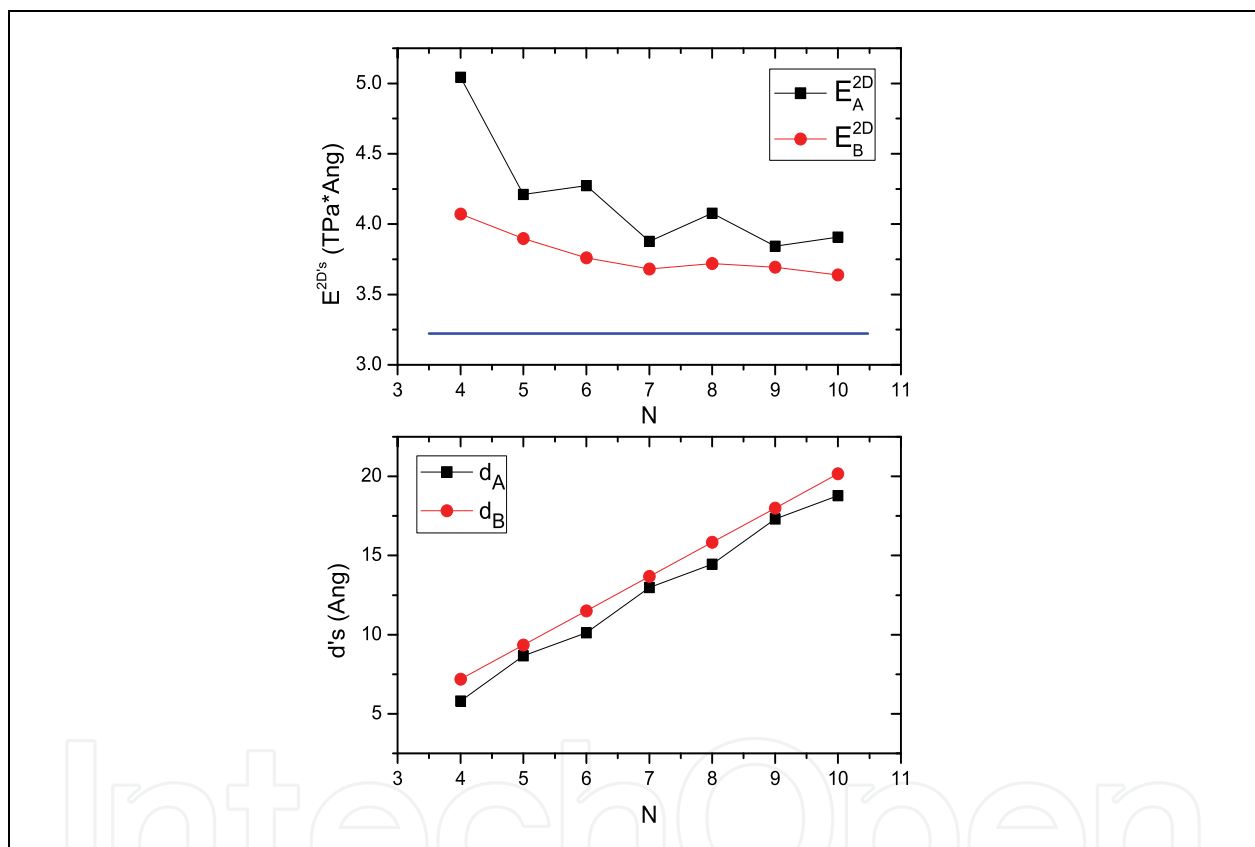Table 3. Final E^{2D}'s Young modulus obtained from the different GNR width (d_i's)

Fig. 6. The N=5 ZGNR sketching the distances: d_A(square-black) and d_B (circle-red); and the E^{2D}'s Young modulus according to the different distances considered in the model which are expressed in terms of the ribbon's width (N). The horizontal blue line corresponds to the graphene results.

The results show E^{2D}_A and E^{2D}_B decreases while N increases, always having a Young's modulus higher than the graphene one. We can argue that ZGNR are harder than graphene. This tendency is the opposite of the case for carbon nanotubes, and the reason can be easily explained in terms of graphene bending. The curvature of CNTs softens the rolled-up graphene sheet because of the lost of overlapping between of the sp^2 orbitals, with a pronounced effect for smaller tubes (Bogár et al. 2005). In the case of GNR the sheet is always plane, with a perfect sp^2 overlapping and strong stiffness. At first, this result would

not be expected, but the response could be understood qualitatively in terms of two opposing effects: the curvature of graphene and geometrical edge reconstruction. The highest curvature corresponds with the lowest the orbital overlap, and hence with the lowest hardness. Furthermore our results indicate that the energy necessary to deform the ribbons (strain energy), expressed as energy per atom, is lower when more carbon atoms are involved, thus fewer atoms hardness of the material. The origin of this effect lies in the geometrical reconstruction of the C-C bonds positioned at the edge. As was mentioned in the introduction, the diagonal C-C distances of GNT at the edges contracts ~ 0.02 Å at the same time that the zigzag C-C-C angle increases ~2°, orientating the stronger C-C diagonal bonds more parallel to the periodic direction of the nanostructure and hardening the bonds. This effect is more evident in the case of thin GNR since there are few C-C bulk bonds, and as the GNR width increases, the bulk bonds prevails diluting the effect of the harder C-C bonds at the edge. In the case of nanotubes the relaxation effect on the edge does not exist, and therefore the curvature effect prevails.
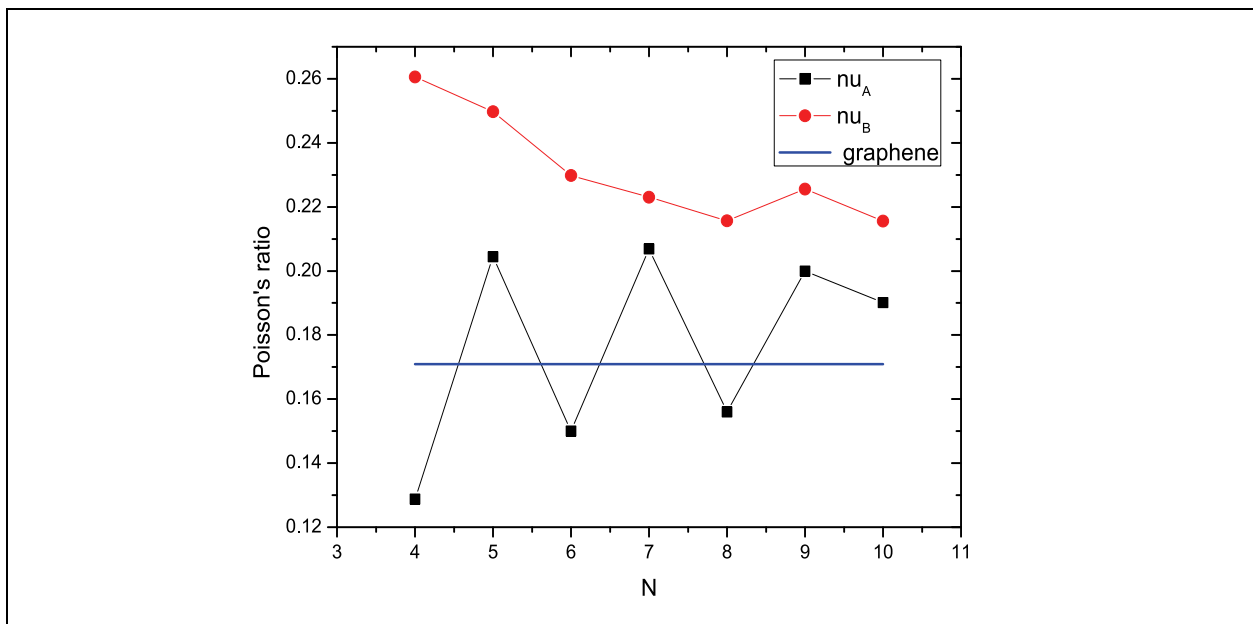

Fig. 7. The υ's dependence upon the GNR's width (N). The horizontal blue line corresponds to graphene results.

The Poisson's ratio presents a similar tendency to the one observed for the Young's modulus. The results are shown in Figure 7 and Table 4, where the (i=A & B) values are presented together with the value for graphene. The tendency between υ and N corresponds to a damped oscillation in the case of υ_A, while the dependency is smoother for the case of υ_B. In an extrapolated limit the infinite widths the ratios υ_i are: $\upsilon_A= 0.18$ and $\upsilon_B= 0.22$.

As was expressed in section 2, the shear modulus (G^{3D}), can be obtained employing equation 1.4 and taken the calculated values for Young's modulus and the Poisson's ratio. For graphene we obtained $G^{3D}= 0.408$ TPa. This value agrees with $G^{3D}=0.384$ TPa reported by Reddy et al. (Reddy et al. 2006), but differs in almost two times with those reported for Sakhaee-Pour (Sakhaee-Pour et al. 2009). Employing a force field method for finite graphene sheets, with different edge terminations, he obtained G values that range from 0.21 to 0.23 TPa. It is important to note that the corresponding Poisson's ratio reported by Sakhaee-Pour was obtained using equation 1.4. However our results are more similar to those reported for

N	υ_A	υ_B	G_A	G_B
4	0.129	0.261	0.667	0.482
5	0.204	0.250	0.522	0.466
6	0.150	0.230	0.555	0.456
7	0.207	0.223	0.480	0.449
8	0.156	0.216	0.526	0.457
9	0.200	0.226	0.478	0.450
10	0.190	0.216	0.490	0.447
∞	0.179		0.408	

Table 4. Poisson's ratio and estimated shear modulus for d_A and d_B models

SWCNT (Li et al. 2003; Tserpes et al. 2005) for which there have been reported G^{3D} values ranging from 0.250 to 0.485 TPa. This is a valid reference for our results, since in this case the mechanical load involves only a single graphene layer. This is the main reason why shear modulus of SWCNT are higher than MWCNT, since in this last case there exist sliding effect between nanotubes that reduces the shear modulus. In one hand, this discrepancy can be attributed to the different nature of the methods used for the simulation. On the other hand our results were estimated for two independent parameters, assuming equation 1.4 being valid. Regarding the dependence of shear modulus upon ribbon width, see Figure 8 and Table 4, what we found is a similar dependence to Young's modulus vs. N. This is an expected result since equation 1.4 is dominated by its numerator, corresponding to the Young's modulus, while the denominator remains almost constant, since the Poisson's ratio remains almost constant. Further simulations, including shear deformation, should be done in order to shed more light on this subject.

Regarding electronic structure features of GNR we found no significant dependence of its properties upon strain. These results agree to those early reported (see Table 1.), whereas for the case of zigzag GNRs it has been found a small variation of energy gaps and local magnetic moments, with no variation in the ordering of the occupied-bands. In our case the energy gaps increases in δE_{gap}=0.02 eV for a positive strain of ε= 0.02, and reduces in δE_{gap}= -0.02 eV for compressive strain ε= -0.02. These results are valid for all the studied GNR's widths. Similar results are obtained for local magnetic moments at the carbon edges, in all the cases the variation are in the order of ± 3% for the same strain range studied.

4. Conclusions

In summary, the electronic and mechanical properties of stressed ZGNR were calculated using *Ab initio* Density Functional Theory. The proposed models allowed us to obtain the corresponding Young's modulus, shear modulus and Poisson's ratio for ZGNR with different width. In all the cases the GNR present higher constants than graphene, but they approximate to this value when the GNR's width is increased. All of this indicates that the narrowest GNR could be one of the strongest materials. This effect could be explained in terms of the hardness of the C-C bonds positioned at the edges of the GNR, due to observed geometrical reconstruction. This property could lead to important consequences regarding the structure of the edge of this nanostructure because chemical substitution, the appearance of defects, and chemical doping could soft or stiff the edges. All these possibilities could lead to an important variation of the mechanical properties of GNR, in particular for the case of shorter GNR of low dimensional systems. It would be interesting to simulate the presence
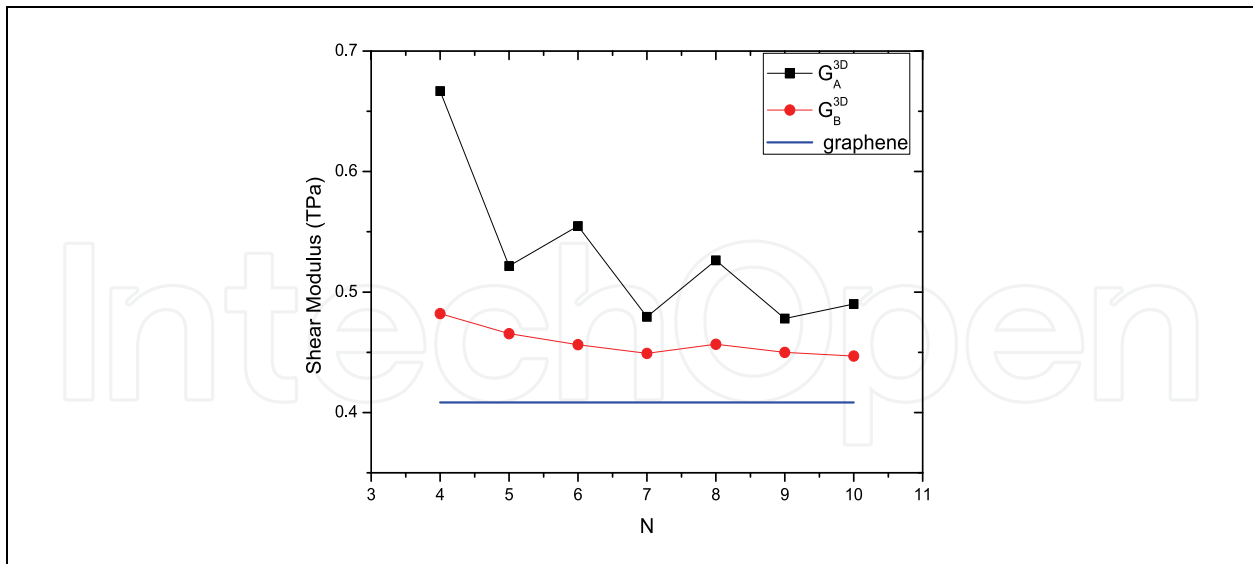
Fig. 8. Shear modulus G3D for GNR indicating the estimated value for graphene.

of strong donating and strong acceptor groups as functional groups substituting the presence of the single H atoms. Regarding the mechanical properties it has been observed a first order dependency of stress upon strain in the region from $\varepsilon = -0.02$ to $\varepsilon = +0.02$. A non-linear dependence is found for higher strain. Electronic structure features are not sensitive to strain in this linear elastic regime, being an additional promise for the using of carbon nanostructures in nano-electronic devices in the near future.

5. Acknowledgments

## 6. References

Arroyo, M. & Belytschko, T. (2004). Finite crystal elasticity of carbon nanotubes based on the exponential Cauchy-Born rule. *Phys. Rev. B*, 69, 115415.

Becke, A. D. (1993). Density-functional thermochemistry. III. The role of exact exchange. *J. Chem. Phys.*, 98, 5648.

Bekyarova, E.; Itkis, M. E.; Ramesh, P.; Berger, C.; Sprinkle, M.; de Heer, W. A.; Haddon, R. C. (2009). Chemical Modification of Epitaxial Graphene: Spontaneous Grafting of Aryl Groups. *J. Am. Chem. Soc.*, 131(4), 1336-1337.

Blakslee, O. L. (1970). *J. Appl. Phys.*, 41, 3373.

Bogár, F.; Mintmire, J. W.; Bartha, F.; Mezo, T. & Van Alsenoy, C. (2005). Density-functional study of the mechanical and electronic properties of narrow carbon nanotubes under axial stress. *Phys. Rev. B*, 72, 085452.

Campos-Delgado, J.; Romo-Herrera, J. M.; Jia, X. T.; Cullen, D. A.; Muramatsu, H.; Kim, Y. A.; Hayashi, T.; Ren, Z. F.; Smith, D. J.; Okuno, Y.; Ohba TKanoh, H.; Kaneko, K.; Endo, M.; Terrones, H.; Dresselhaus, M. S. &Terrones, M. (2008). Bulk production of a new form of sp(2) carbon: Crystalline graphene nanoribbons. *Nano Letters*, 8 (9), 2773-2778.

Ceperley, D. M. and Alder, B. J. (1980). Ground State of the Electron Gas by a Stochastic Method. *Phys. Rev. Lett.*, 45, 566-569.

Charlier, J.-C.; Gonze, X. & Michenaud, J.-P. (1994). First-principles study of the stacking effect on the electronic properties of graphite(s). *Carbon*, 32, 289-299.

Denis, P. A.; Faccio, R. (2008). Theoretical characterization of thioepoxidated single wall carbon nanotubes. *Chem. Phys Lett.*, 460, 486-491.

Denis, P. A.; Faccio, R.; Mombrú, A. W. (2009). Is It Possible to Dope Single-Walled Carbon Nanotubes and Graphene with Sulfur? *ChemPhysChem,* 10, 715-722.

Dion, M.; Rydberg, H.; Schröder, E.; Langreth, D. C. & Lundqvist, B. I. (2004). Van der Waals Density Functional for General Geometries. *Phys. Rev. Lett.*, 92, 246401.

Faccio, R.; Pardo, H.; Denis, P.A.; Yoshikawa-Oreiras, R.; Araújo-Moreira, F. M.; Verisimo-Alves, M. & Mombrú, A. W. (2008). Magnetism induced by single carbon vacancies in a three-dimensional graphitic network. *Phys. Rev. B.*, 77, 035416.

Faccio, R.; Denis, P.; Pardo, H.; Goyenola, C. & Mombrú, A. W. (2009). Mechanical properties of graphene nanorribons. *J. Phys: Cond. Matt.*, 21(8), 285304.

Friesecke, G. & Theil, F. (2002). Validity and failure of the Cauchy-Born hypothesis in a two-dimensional mass-spring lattice. *J. Nonlinear Sci.*, 12, 445-478.

Fujita, M.; Wakabayashi, K.; Nakada, K. & Kusakabe, K. (1996). Peculiar Localized State at Zigzag Graphite Edge. *J. Phys. Soc. Jpn.*, 65, 1920-1923.

Gui, G.; Li, J. & Zhong, J. (2008). Band structure engineering of graphene by strain: First-principles calculations. *Phys. Rev. B*, 78, 075435.

Hoheisel, T. N.; Schrettl, S.; Szilluweit, R. & Frauenrath, H. (2010). Nanostructured Carbonaceous Materials from Molecular Precursors. *Angew. Chem. Int. Ed.*, 49, 6496 – 6515

Hohenberg, P. & Kohn, W. (1964). Inhomogeneous Electron Gas. *Phys. Rev.*, 136, B864-B871.

Khare, R.; Mielke, S. L.; Paci, J. T.; Zhang, S.; Ballarini, R.; Schatz, G. C. & Belytschko, T. (2007). Coupled quantum mechanical/molecular mechanical modeling of the fracture of defective carbon nanotubes and graphene sheets. *Phys. Rev. B*, 75, 075412.

Kohn, W. & Sham, L. J. (1965). Self-Consistent Equations Including Exchange and Correlation Effects. *Phys. Rev.,* 140, A1133-A1138.

Khon, W.; Meir, Y. & Makarov, D. E. (1998). van der Waals Energies in Density Functional Theory. *Phys. Rev. Lett.*, 80, 4153-4156.

Kohanoff, J. and Gidopoulos, N. I. (2002). Density Functional Theory: Basics, New Trends and Applications - The Handbook of Molecular Physics and Quantum Chemistry, Ed. S. Wilson, Molecular Electronic Structure, John Wiley & Sons, ISBN 0471623741, Chichester.

Konstantinova, E.; Dantas, S. O. & Barone, P. M. V. B. (2006). Electronic and elastic properties of two-dimensional carbon planes. *Phys. Rev. B*, 74, 035417.

Kudin, K. N.; Scuseria, G. E. & Yakobson, B. I. (2001). C_2F, BN, and C nanoshell elasticity from *Ab initio* computations. *Phys. Rev. B*, 64, 235406.

Lee, C.; Yang, W. & Parr, R. G. (1988). Development of the Colle-Salvetti correlation-energy formula into a functional of the electron density. *Phys. Rev. B*, 37, 785-789.

Lee, C.; Wei, X.; Kysar, J. W.; Hone, J. (2008). Measurement of the Elastic Properties and Intrinsic Strength of Monolayer Graphene. *Science,* 321, 385-388.

Li, C.; Chou, T.-W. (2003). A structural mechanics approach for the analysis of carbon nanotubes. Int. J. Solid Struct., 40, 2487-2499.

Lier, G. V.; Alsenoy, C. V.; Doren, V. V. & Greelings, P. (2000). *Ab initio* Study of the Elastic Properties of Single-Walled Carbon Nanotubes and Graphene". *Chem. Phys. Lett.*, 326, 181.

Liu, F.; Ming, P. M. & Li, J. (2007). *Ab initio* calculation of ideal strength and phonon instability of graphene under tension. *Phys. Rev. B*, 76, 064120.

Lu, J. P. (1997). Elastic Properties of Carbon Nanotubes and Nanoropes. *Phys. Rev. Lett.*, 79, 1297-1300.

Miyamoto, Y.; Nakada, K. & Fujita, M. (1999). First-principles study of edge states of H-terminated graphitic ribbons. *Phys. Rev. B*, 59, 9859.

Monkhorst, H. J. & Pack, J. D. (1976). Special points for Brillouin-zone integrations. *Phys. Rev. B*, 13, 5188-5192.

Nakada, K.; Fujita, M.; Dresselhaus, G. & Dresselhaus, M. S. (1996). Edge state in graphene ribbons: Nanometer size effect and edge shape dependence. *Phys. Rev. B*, 54, 17954.

Ordejón, P.; Artacho, E. & Soler, J.M. (1996). Self-consistent order-N density-functional calculations for very large systems. *Phys. Rev. B*, 53, R10441

Palacio, F. & Makarova, T. (2005). *Carbon-based Magnetism,* ISBN 13:978.0.444.51947-4, Elsevier. B. V., Amsterdam, The Netherlands.

Perdew, J. P. and Zunger, A. (1981). Self-interaction correction to density-functional approximations for many-electron systems. *Phys. Rev. B*, 23, 5048-5079.

Perdew, J. P.; Burke, K.; and M. Ernzerhof, (1996). Generalized Gradient Approximation Made Simple. Phys. Rev. Lett., 77, 3865;

Perdew, J. P.; Burke, K.; and M. Ernzerhof (1997). Generalized Gradient Approximation Made Simple [Phys. Rev. Lett. 77, 3865 (1996)]. Phys. Rev. Lett., 78, 1396-1396.

Pereira, V. M.; Castro Neto, A. H. & Peres, N. M. R. (2009). Tight-binding approach to uniaxial strain in graphene. *Phys. Rev. B*, 80, 045401.

Press, W. H.; Flannery, B. P.; Teukolsky, S. A.; Vetterling, W. T. (1986). *New Numerical Recipes*, Cambridge University Press, New York.

Pisani, L.; Chan, J.A.; Montanari, B. & Harrison, N.M. (2007). Electronic structure and magnetic properties of graphitic ribbons. *Phys. Rev. B*, 75, 064418.

Reddy, C. D.; Rajendran, S. & Liew, K. M. (2005). Equivalent continuum modeling of graphene sheet. *Int. J. Nanosci.*, 4, 631-636.

Reddy, C. D.; Rajendran, S. & Liew, K. M. (2006).Equilibrium configuration and elastic properties of finite graphene. *Nanotechnology*, 17, 864-870.Xu, Z. (2009). Graphene Nano-Ribbons Under Tension. *Journal of Computational and Theoretical Nanoscience*, 6, 1-3.

Román-Pérez, G. & Soler, J. M. (2009). Efficient Implementation of a van der Waals Density Functional: Application to Double-Wall Carbon Nanotubes. *Phys. Rev. Lett.*, 103, 096102.

Rydberg, H.; Dion, M.; Jacobson, N.; Schröder, E.; Hyldgaard, P.; Simak, S. I.; Langreth, D. C. & Lundqvist, B. I. (2003). Van der Waals Density Functional for Layered Structures. *Phys. Rev. Lett.*, 91, 126402.

Sakhaee-Pour, A. (2009). Elastic properties of single-layered graphene sheet. *Solid State Communications*, 149, 91-95.

Sammalkorpi, M.; Krasheninnikov, A.; Kuronen, A.; Nordlund, K. & Kaski, K. (2004) Mechanical properties of carbon nanotubes with vacancies and related defects. Phys. Rev. B 70, 245416.

Sánchez-Portal, D.; Ordejón, P.; Artacho, E.; Soler, J.M. (1997). Density-functional method for very large systems with LCAO basis sets. *Int. J. Quantum Chem.*, 65, 453-461.

Shen, L. & Li, J. (2004). Equilibrium structure and strain energy of single-walled carbon nanotubes. *Phys. Rev. B*, 69, 045414.

Soler, J. M.; Artacho, E.; Gale, J.; D. García, A.; Junquera, J.; Ordejón, P.; Sánchez-Portal, D. (2002). The SIESTA method for *Ab initio* order-N materials simulation. *J. Phys.: Condens. Matter*, 14, 2745-.

Stephens, P. J.; Devlin, F. J.; Chabalowski, C. F. & Frisch, M. J.(1994). *Ab initio* Calculation of Vibrational Absorption and Circular Dichroism Spectra Using Density Functional Force Fields. *J. Phys. Chem.*, 98, 11623-11627.

Strocov, V. N.; Blaha, P.; Starnberg, H. I.; Rohlfing, M.; Claessen, R.; Debever, J.-M. & Themlin, J.-M. (2000). Three-dimensional unoccupied band structure of graphite: Very-low-energy electron diffraction and band calculations. *Phys. Rev. B*, 61, 7, 4994-5001.

(a) Son, Y.-W.; Cohen, M. L. & Louie, S. G. (2006). Half-metallic graphene nanoribbons. *Nature* (London) 444, 347-349.

(b) Son, Y.-W.; Cohen, M. L. & Louie, S. G. (2006). Energy Gaps in Graphene. *Phys. Rev. Lett.* 97, 216803.

Su, W. S.; Wu, B. R. & Leung, T. C. (2008). The Deformation Effect on the Electronic Structure of the Graphite Nanoribbon Arrays, *cond-mat*/0810.4582

Sun, L.; Li, Q.; Ren, H.; Su, H.; Shi, Q. W. & Yang, J. (2008). Strain effect on electronic structures of graphene nanoribbons: A first-principles study. *J. Chem. Phys.*, 129, 074704.

Tournus, F. ; Charlier, J. C. ; Mélinon, P. (2005). Mutual orientation of two C60 molecules : an *Ab initio* study. *J. Chem. Phys.*, 122, 094315.

Troullier, N.; Martins, J.L. (1991).Efficient pseudopotentials for plane-wave calculations. *Phys. Rev. B*, 43, 1993-2006.

Trucano, P. & Chen, R. (1975). Structure of graphite by neutron diffraction. *Nature (London)*, *258*, 136-137.

Tserpes, K. I.; Papanikos, P. (2005). Composites Part B: Engineering, 36(5), 468-477.

Vosko, S. H.; Wilk, L. & Nusair, M. (1980). Accurate spin-dependent electron liquid correlation energies for local spin density calculations: a critical analysis". *Can. J. Phys.*, 58(8), 1200-1211.

Wakabayashi, K.; Fujita, M.; Ajiki, H. & Sigrist, M. (1999). Electronic and magnetic properties of nanographite ribbons. *Phys. Rev. B*, 59, 8271.

Wirtz, L. & Rubio, A. (2004). The phonon dispersion of graphite revisited. *Solid State Communications*, 131, 141-152.

Wu, Y.; Huang, M.; Wang, F.; Henry Huang, X. M.; Rosenblatt, S.; Huang, L.; Yan, H.; O'Brien, S. P.; Hone, J. & Heinz, T. F. (2008). Determination of the Young's Modulus of Structurally Defined Carbon Nanotubes. *Nano Letters*, 8(12), 4158–4161.

Yoon, J.; Ru, C. Q. & Mioduchowski, A. (2005). Terahertz Vibration of Short Carbon Nanotubes Modeled as Timoshenko Beams. *J. Appl. Mech.*, 72(1), 10-17.

Yu, M. F.; Files, B. S.; Arepalli, S. & Ruoff, R. S. (2000). Tensile Loading of Ropes of Single Wall Carbon Nanotubes and their Mechanical Properties. *Phys. Rev. Lett.*, 84, 5552-5555.

Zhang, P.; Jiang, H.; Huang, Y.; Geubelle, P. H. & Hwang, K. C. (2002). The elastic modulus of single-wall carbon nanotubes: a continuum analysis incorporating interatomic potentials. Int. J. Solids Struct. 39, 3893-3906.

Zhang, Y.; Talapatra, S.; Kar, S.; Vajtai, R.; Nayak; S. K. and Ajayan, P. M. (2007). First-Principles Study of Defect-Induced Magnetism in Carbon. *Phys. Rev. Lett.*, 99, 107201.
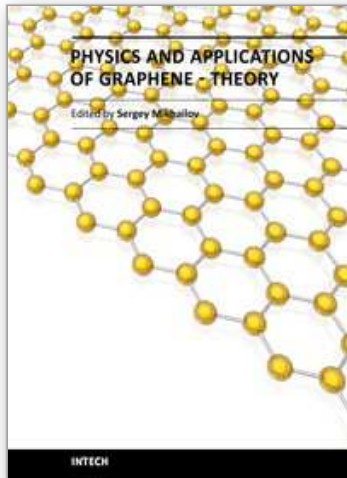
Physics and Applications of Graphene - Theory

Edited by Dr. Sergey Mikhailov

The Stone Age, the Bronze Age, the Iron Age... Every global epoch in the history of the mankind is characterized by materials used in it. In 2004 a new era in material science was opened: the era of graphene or, more generally, of two-dimensional materials. Graphene is the strongest and the most stretchable known material, it has the record thermal conductivity and the very high mobility of charge carriers. It demonstrates many interesting fundamental physical effects and promises a lot of applications, among which are conductive ink, terahertz transistors, ultrafast photodetectors and bendable touch screens. In 2010 Andre Geim and Konstantin Novoselov were awarded the Nobel Prize in Physics "for groundbreaking experiments regarding the two-dimensional material graphene". The two volumes Physics and Applications of Graphene - Experiments and Physics and Applications of Graphene - Theory contain a collection of research articles reporting on different aspects of experimental and theoretical studies of this new material.

How to reference

In order to correctly reference this scholarly work, feel free to copy and paste the following:

Ricardo Faccio, Luciana Fernández-Werner, Helena Pardo, Cecilia Goyenola, Pablo A. Denis and Álvaro W. Mombrú (2011). Mechanical and Electronic Properties of Graphene Nanostructures, Physics and Applications of Graphene - Theory, Dr. Sergey Mikhailov (Ed.), ISBN: 978-953-307-152-7, InTech, Available from: http://www.intechopen.com/books/physics-and-applications-of-graphene-theory/mechanical-and-electronic-properties-of-graphene-nanostructures

INTECH

open science | open minds